JMEPEG (2012) 21:1998–2001
DOI: 10.1007/s11665-011-0113-z

1059-9495/$19.00

Effect of MnO_2 Addition on Sintering Properties of 18NiO-$NiFe_2O_4$ Composite Ceramics: Preliminary Results

Jinjing Du, Yihan Liu, Guangchun Yao, and Zhigang Zhang

(Submitted March 1, 2011; in revised form December 12, 2011)

$NiFe_2O_4$ samples with small amounts of MnO_2 were prepared via ball-milling process and two-step sintering process from commercial powders. Sintered density, average grain size, and microstructure of Mn-doped 18NiO-$NiFe_2O_4$ composite ceramics have been investigated by means of x-ray diffraction, scanning electron microscopy, and energy dispersive spectroscopy. Bending strength was measured by three-point method. The results show that the crystalline structures of the ceramic matrix are still $NiFe_2O_4$ spinel structure and Mn ions homogeneously distribute in both the grains interiors and the grain boundaries. When 1 wt.% MnO_2 was added, the values of relative density and bending strength of composite ceramics reached their respective maximum of 93.6% and 38.75 MPa, respectively. It is preliminarily found that MnO_2 can reduce the sintering temperature obviously because of partial substitution of Fe^{3+} with Mn^{4+} in $NiFe_2O_4$ lattice.

Keywords ceramic matrix composites, grain refinement, heat treating, mechanical testing, MnO_2 addition

The novel techniques of aluminum electrolysis with inert anodes have been an important item for many years (Ref 1, 2). The development of green anode materials has gained considerable importance in recent years (Ref 3). At present, the current efficiency of aluminum electrolysis is as high as 96%, but consumable carbon anodes are used, the anode product being CO_2 and CO (Ref 4).

Relatively extensive researches have been carried out to develop a suitable material served as inert anodes to replace commonly used carbon anodes, which would solve numerous ecological and economical problems by releasing environment-friendly O_2 during electrolysis (Ref 5-8). It is found that $NiFe_2O_4$-based cermets are one of the most promising candidates served as inert anodes for aluminum electrolysis, which possess a better corrosion resistance and higher thermal shock resistance in molten cryolite-alumina bath (Ref 9-11).

However, low reactivity of solid substance in the preparation of ceramic matrix will result in a slower reaction rate, so it is hard to obtain high-density target products at low temperatures (Ref 12). In order to obtain high-density target products at lower temperature, two common methods, either preparing ultrafine powder or using sintering promoters, have been exploited (Ref 12-14). It is more economical to adopt sintering promoters to improve sintering ability for large-scale fabrication (Ref 15, 16). Zhang et al. (Ref 17) reported that a relative density of ~68% was obtained for pure ceramics sintered at 1300 °C for 1 h. However, a relative density of ~94% was gained for 1 wt.% MnO_2-doped samples at the same sintering conditions. Densities of alumina samples sintered at 1550 °C for 1 h can reach 95% of the theoretical density (TD). The densities of those containing 3.0% MnO_2 and 0.5% TiO_2 sintered at 1250 °C for 1 h are up to 98.2% of the TD (Ref 18). It can be seen that sintering promoters is useful for some solid-state sintering and MnO_2 is an effective sintering promoter for certain ceramic materials mentioned above.

In this study, high-purity reagents (Fe_2O_3: 99.3%, NiO: 99.98%, MnO_2: 97.5%; Guoyao, China) are selected as raw materials. A two-step sintering process was adopted to prepare MnO_2-doped $NiFe_2O_4$ composite ceramics. The molar ratio of NiO to Fe_2O_3 was 1.87:1 in the mixture. Powder mixtures of NiO and Fe_2O_3 were ground in distilled water via a ball-milling process for 24 h and dried. Then the mixtures were ground with 4 vol.% polyvinyl alcohol (PVA) binder and pressed at 160 MPa into rectangular bars. The ceramic bars were calcined in air at 1000 °C for 6 h to produce $NiFe_2O_4$ matrix material. The calcined matrix products were crushed and ball-milled with different amounts of MnO_2 (i.e., $x = 0$, 0.5, 1.0, 1.5, 2.0, 2.5 wt%) for another 24 h with distilled water as dispersant, then dried thoroughly. Adding 4 vol.% PVA binder, the dried mixture was fabricated into $70 \times 15 \times 8$ mm ceramic bars at a pressure of 200 MPa and then sintered at 1100, 1200, 1300, 1400 °C for 6 h in air, respectively, to produce 18%NiO-$NiFe_2O_4$ composite ceramics.

Bulk density and porosity of sintered samples were tested by Archimedes drainage. Bending strength was measured by three-point method using an electron mechanical experimental machine (USA). Fracture surface and well-polished surface of sintered samples were characterized using scanning electron microscope (SSX-550, Japan). The phase transformation in sintered samples was detected using a D/max 2RB x-ray diffractometer (Japan) with Cu Kα radiation, pip voltage 40 kV

Jinjing Du, Yihan Liu, Guangchun Yao, and **Zhigang Zhang,** School of Materials and Metallurgy, Northeastern University, P.O. Box 117, Shenyang 110004, China. Contact e-mail: djzneu@yahoo.cn.

and current 100 mA. The elemental analysis in sintered samples was carried out using energy dispersive x-ray microanalysis (EDAX).

The XRD patterns of un-doped and 2.0 wt.% MnO_2-doped samples are shown in Fig. 1. As shown in Fig. 1, all samples are identified to be cubic spinel structure with most intense peak (3 1 1), which indicate that no new phases formed in the sintered samples. According to research work by Yao et al. (Ref 19), after introduction of 2.0 wt.% MnO_2 into the ceramic matrix, a formation of solid solution caused by MnO_2 and $NiFe_2O_4$ could be detected in the samples. Figure 1(b) indicates that Mn ions entered the crystal lattice of $NiFe_2O_4$. As the valence of ion Mn^{4+} is higher than that of Fe^{3+}, Mn^{4+} entered the octahedron positions of $NiFe_2O_4$ spinel and partially substituted Fe^{3+} (Ref 20). It produced ion vacancy in the lattice of $NiFe_2O_4$. So the crystal lattice of $NiFe_2O_4$ is distorted by Mn^{4+} entrance, although it still retains its $NiFe_2O_4$ spinel structure. All the radii of the ions in sintered samples are shown in Table 1.

In general, the ions with higher valence and larger radii are prone to occupy the octahedron positions and the ions with lower valence and smaller radii are prone to occupy the tetrahedron positions (Ref 21). Based on the above-mentioned reasons, Mn^{4+} ions have the preference to occupy octahedron positions of $NiFe_2O_4$ spinel. It is in good agreement with the description by Zhang et al. (Ref 20, 22)and Bonsdorf et al. (Ref 20, 22). MnO_2 addition shifts the value of the lattice constant towards higher tendency from 8.31 for un-doped samples to 8.341 for 2.0 wt.% MnO_2-doped samples (Ref 20). It is proved the lattice distortion in $NiFe_2O_4$ spinel caused by substitution of partial Fe^{3+} by Mn^{4+} ions.

Selected micrographs, as shown in Fig. 2, indicate the grains of un-doped ceramic samples sintered at 1300 °C are not strongly bonded together. Plenty of pores can be found (Fig. 2a). When 0.5 wt.% MnO_2 was added, apparent sintering trajectories can be detected in the samples sintered at 1200 °C (Fig. 2b). It is interesting to note that solid-solution phenomenon happened in 1 wt.% MnO_2-doped samples sintered at 1200 °C. Moreover the grain size is smaller than that shown in Fig. 2(a), (b). The possible reason is that 1 wt.% MnO_2 is effective for controlling abnormal grain growth through a solid-solution pinning mechanism and thus, achieving higher densities along with uniform structure. When MnO_2 content is up to 2.5 wt.%, the distribution of particle size is not uniform, local positions are riddled with pores and structure is not as dense as that of 1 wt.% MnO_2-doped samples. It can be understood that entrance of excessive Mn^{4+} ions into the lattice of $NiFe_2O_4$ leads to unbalance distribution of Fe ions. It will attenuate the super-exchange interactions of Fe^{3+} ions between A site and B site, which results in hard displacement of domain wall and MnO_2 segregation at grain boundaries. It should be possible to increase the diffusion activation energy and decrease the diffusion rate, which is unfavorable for sintering process.

The selected morphology of samples and corresponding distribution of Mn element is shown in Fig. 3. It is observed that Mn element is homogeneously distributed on the analyzed region. It can be concluded that most Mn element is dissolved both in the $NiFe_2O_4$ spinel grains and in the grain boundaries. It is clear that Mn element probably form a solid solution with the synthesized $NiFe_2O_4$ spinel, which is consistent with the observation in Fig. 1(b).

The lattice spacing d of samples with different crystal face indexes for un-doped and 1 wt.% MnO_2-doped samples are listed in Table 2. It is indicated that the d values for 1 wt.% MnO_2-doped samples are smaller than those of un-doped samples. It is illustrated that MnO_2 additive does lead to the deviation of lattice parameter in $NiFe_2O_4$ spinel.

Relative densities and bending strengths of samples sintered at 1200 °C for 6 h with different amounts of MnO_2 are described in Fig. 4. It can be seen that un-doped samples have a lower relative density (~90.84%) and poorer bending strength (~19.03 MPa). Increasing MnO_2 doping content from 0 to 1 wt.%, the both values increase and reach a maximum at x = 1.0 wt.%. When the amount of MnO_2 doping is over 1.0 wt/%, the values of both relative density and bending strength decrease and get to a minimum at about x = 2.5 wt.%. It can be concluded that a lower doping level (< 1 wt.%) is effective in promoting densification, while a higher doping level (> 1 wt.%) is ineffective in this study. A similar effect of MnO_2 additive on densification of CeO_2 has been proved by Zhang et al. (Ref 15, 17).

Table 1 The radii of the ions in the sintered samples

Element	Mn^{2+}	Mn^{3+}	Mn^{4+}	Fe^{3+}	Ni^{2+}	O^{2-}
Ionic radii, nm	0.091	0.066	0.052	0.064	0.068	0.14

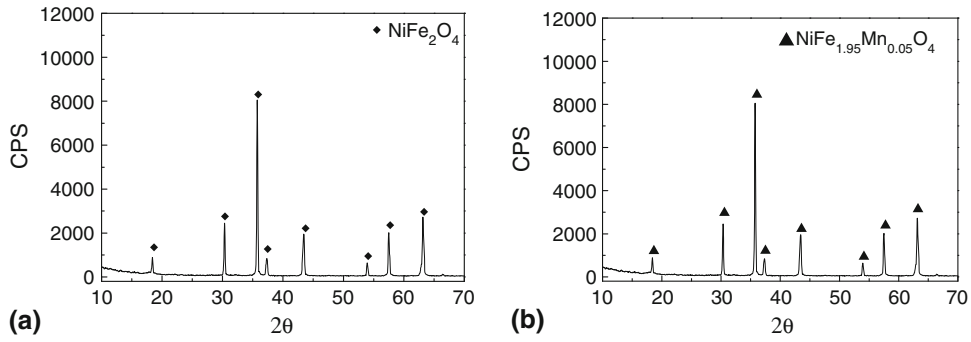

Fig. 1 XRD patterns of samples sintered at 1200 °C for 6 h in air. (a) Without MnO_2 and (b) with 2.0 wt.% MnO_2 additive

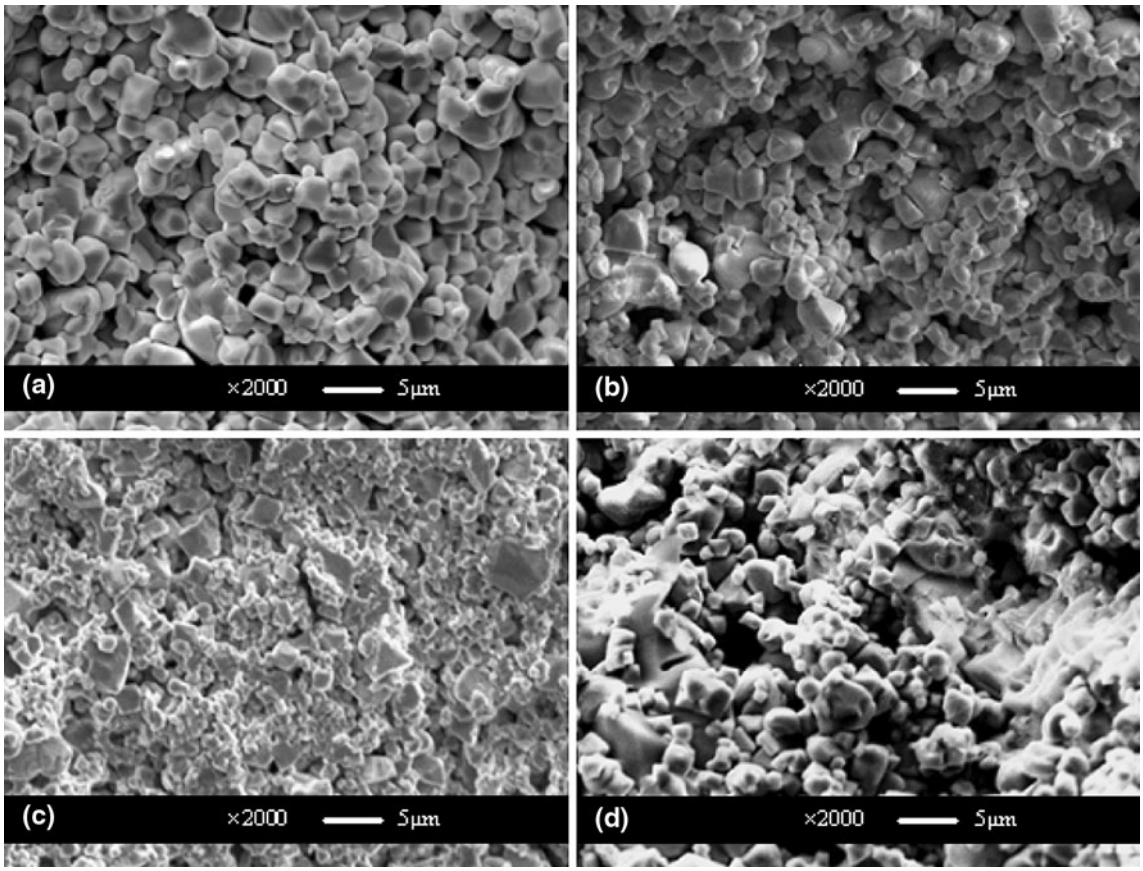

Fig. 2 SEM micrographs of the ceramic samples: (a) x = 0% (i.e., without MnO_2 additive), sintered at 1300 °C for 6 h; (b) x = 0.5 wt.%, sintered at 1200 °C for 6 h; (c) x = 1.0 wt.%, sintered at 1200 °C for 6 h; (d) x = 2.5 wt.%, sintered at 1200 °C for 6 h

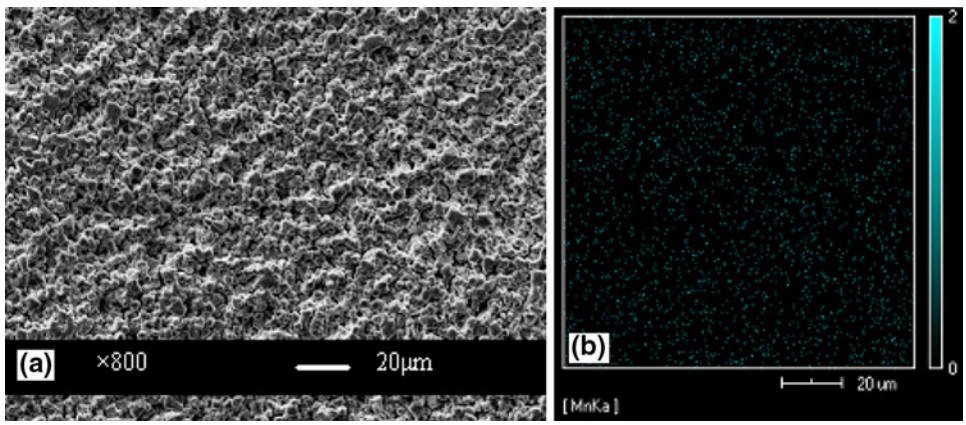

Fig. 3 (a) SEM image of the ceramic samples doped with 1.0 wt.% of MnO_2 and (b) the distribution of Mn element in the ceramic samples with 1.0 wt.% MnO_2

All the results indicated that the crystalline structures of MnO_2-doped ceramic matrix are still $NiFe_2O_4$ spinel structure. Mn element distributes homogeneously in both the grains interiors and the grain boundaries of $NiFe_2O_4$ spinel. Introduction of MnO_2 makes it easier to obtain a dense $NiFe_2O_4$ ceramic with smaller grain size. It is suggested that proper amount of MnO_2 addition can decrease the sintering temperature, evidence proving MnO_2 is an effective sintering additive for getting denser $NiFe_2O_4$. The values of both the relative density and the bending strength for 1.0 wt.% MnO_2-doped samples reached their respective maximum of 93.6% and 38.75 MPa. In addition, introduction of excessive MnO_2 additive to the ceramic matrix will be unfavorable for the sintering, i.e., 2.5 wt.% MnO_2 in this article.

Table 2 The values of interplanar spacing *d* for the sintered samples with different crystal face indexes

	Lattice spacing *d*, nm	
hkl	**$NiFe_2O_4$**	**1 wt.% MnO_2-$NiFe_2O_4$**
111	0.483097	0.481795
220	0.295218	0.294742
311	0.251541	0.251300
222	0.240880	0.240880
400	0.208560	0.208332
422	0.170257	0.170110
511	0.160404	0.160277
440	0.147426	0.147217
620	0.131844	0.131685
533	0.127188	0.127042

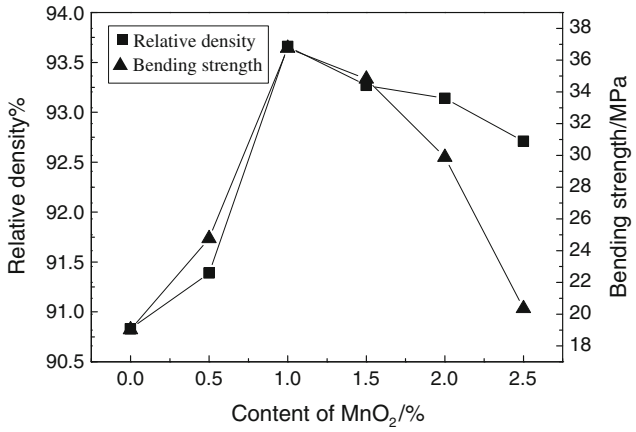

Fig. 4 Relative densities and bending strengths of samples sintered at 1200 °C for 6 h with different amounts of MnO_2

Acknowledgments

The authors gratefully acknowledge the financial support from the State Key Program of National Natural Science of China (No. 50834001) and National High Technology Research and Development Program of China (863 Program) (No. 2009AA03Z502).

References

1. Y.Q. Lai, Y. Zhang, Z.L. Tian, X.G. Sun, G. Zhang, and J. Li, Effect of Adding Methods of Metallic Phase on Microstructure and Thermal Shock Resistance of Ni/(90NiFe2O4-10NiO) Cermets, *Trans. Nonferrous Met. Soc. China*, 2007, **17**, p 681–685
2. J. Keniry, The Economics of Inert Anodes and Wettable Cathodes for Aluminum Reduction Cells, *J. Manag.*, 2001, **53**(5), p 43–47
3. L.J. Berchmans, R.K. Selvan, and C.O. Augustin, Evaluation of Mg^{2+}-Substituted $NiFe_2O_4$ as a Green Anode Material, *Mater. Lett.*, 2004, **58**, p 1928–1933
4. J. Ma, G.C. Yao, L. Bao, X. Zhang, and J.F. Ma, Research on Preparation and properties of 18NiO-$NiFe_2O_4$ composite ceramic inert anodes, *Light Metals*, 2010, p 949–952
5. Y.Q. Lai, Z.L. Tian, J. Li, S.L. Ye, and Y.X. Liu, Preliminary Testing of $NiFe_2O_4$-NiO-Ni Cermet as Inert Anode in Na_3AlF_6-AlF_3 Melts, *Trans. Nonferrous Met. Soc. China*, 2006, **16**, p 654–658
6. J. Thonstad, P. Fellner, G.M. Haarberg, J. Hhts, H. Kvande, and A. Sterten, *Aluminium Electrolysis-Fundamentals of the Hall-Heroult Process*, 3rd ed., Aluminium-Verlag, MI. Dusseldorf, Germany, 2001, p 328–338
7. J.H. Yang, Y.X. Liu, and H.H. Wang, The Behaviour and Improvement of SnO_2-Based Inert Anodes in Aluminium Electrolysis, *Light Metals*, S.K. Das, Ed., TMS, Warrendale, PA, 1993, p 493–495
8. R.D. Peterson, N.E. Richards, and A.T. Tabereaux, Results of 100 Hour Electrolysis Test of a Cermet Anode: Operational Results and Industry Perspective, *Light Metals*, M.B. Christian, Ed., TMS, Warrendale, PA, 1990,
9. S.P. Ray, Inert anodes for Hall cells, *Light Metals*, R.T. Miller, Ed., TMS, Warrendale PA, 1986, p 287–298
10. E. Olsen and J. Thonstad, Nickel Ferrite as Inert Anodes in Aluminium Electrolysis (part I): Material Fabrication and Preliminary Testing, *J. Appl. Electrochem.*, 1999, **29**, p 293–299
11. D.R. Sadoway, Inert Anodes for the Hall Hároult Cell: The Ultimate Materials Challenge, *J. Manag.*, 2001, **53**(5), p 34–35
12. L.M. Zhang, X.H. Huang, and X.L. Song, *Fundamentals of Materials Science*, Wuhan University of Technology Press, Wuhan, 2008 (in Chinese)
13. Z.G. Zhang, G.C. Yao, J. Ma, and Z.S. Hua, Synthesis of $NiFe_2O_4$ Spinel Nanopowder via Low-Temperature Solid-State Reactions, *J. Northeast. Univ. (Nat. Sci.)*, 2010, **31**(6), p 868–871 (in Chinese)
14. J.H. Xi, G.C. Yao, Y.H. Liu, and X.M. Zhang, Effects of Additive V_2O_5 on Sintering Mechanism and Properties of Nickel Ferrite, *J. Chin. Ceram. Soc.*, 2005, **33**(6), p 683–687 (in Chinese)
15. T.S. Zhang, P. Hing, H.T. Huang, and J. Kilner, Sintering and Densification Behavior of Mn-Doped CeO_2, *Mater. Sci. Eng. B*, 2001, **83**, p 235–241
16. J.A. Cerri, E.R. Leite, D. Gouvea, and E. Longo, Effect of Cobalt (II) Oxide and Manganese (IV) Oxide on Sintering of Tin (IV) Oxide, *J. Am. Ceram. Soc.*, 1996, **79**, p 799–801
17. T.S. Zhang, P. Hing, H.T. Huang, and J. Kilner, Sintering Study on Commercial CeO_2 Powder with Small Amount of MnO_2 Doping, *Mater. Lett.*, 2002, **57**, p 507–512
18. H. Erkalfa, Z. Misirli, and T. Baykara, Densification of Alumina at 1250°C with MnO_2 and TiO_2 Additives, *Ceram. Int.*, 1995, **21**, p 345–348
19. G.C. Yao, Y.H. Liu et al., *Preparative Technology for Advanced Materials*, Northeastern University Press, Shenyang, 2006
20. X. Zhang, Y.P. Duan, H.T. Guan, S.H. Liu, and B. Wen, Effect of Doping MnO_2 on Magnetic Properties for M-Type Barium Ferrite, *J. Magn. Mater.*, 2007, **311**, p 507–511
21. Z.G. Zhou, *Ferrite Magnetic Materials*, Science Press, Beijing, 1981
22. G. Bonsdorf, M.A. Deneeke, and K. Schafer, X-ray Absorption Spectroscopic and Mössbauer Studies of Redox and Cation-Ordering Processes in Manganese Ferrite, *Solid State Ion.*, 1997, **101**, p 351–357